Contact size scaling of a W-contact phase-change memory cell based on numerical simulation*

Wei Yiqun(魏益群)[1], Lin Xinnan(林信南)[1,†], Jia Yuchao(贾宇超)[1], Cui Xiaole(崔小乐)[1], Zhang Xing(张兴)[1,2], and Song Zhitang(宋志棠)[1,3]

[1]Key Laboratory of Integrated Microsystems, Shenzhen Graduate School of Peking University, Shenzhen 518055, China
[2]TSRC, Key Laboratory of Microelectronic Devices and Circuits, Institute of Microelectronics, School of Electronics and Computer Science, Peking University, Beijing 100871, China
[3]State Key Laboratory of Functional Materials for Informatics, Shanghai Institute of Microsystem and Information Technology, Chinese Academy of Sciences, Shanghai 200050, China

Abstract: In the design of phase-change memory (PCM), it is important to perform numerical simulations to predict the performances of different device structures. This work presents a numerical simulation using a coupled system including Poisson's equation, the current continuity equation, the thermal conductivity equation, and phase-change dynamics to simulate the thermal and electric characteristics of phase-change memory. This method discriminates the common numerical simulation of PCM cells, from which it applies Possion's equation and current continuity equations instead of the Laplace equation to depict the electric characteristics of PCM cells, which is more adoptable for the semiconductor characteristics of phase-change materials. The results show that the simulation agrees with the measurement, and the scalability of PCM is predicted.

Key words: phase-change memory; scaling; numerical simulation
DOI: 10.1088/1674-4926/33/10/104006 **PACC:** 7280; 9160H; 8220W

1. Introduction

Phase-change memory (PCM) is becoming the most promising candidate for the next generation of non-volatile memory due to its high density, high reliability, low power, and compatibility with standard CMOS processes[1−4]. To optimize device structural design and predict device performance, it is necessary to present an accurate numerical simulation. In the past, some simulation methods for PCM cells were proposed, such as ECD and SAMSUNG[5−7]. These methods neglect the semiconductor characteristics of the phase-change material, using Laplace's equation instead of Possion's equation to model the electric characteristics. However, a phase-change material is essentially semiconductor and is more adaptable for simulating the electric characteristics based on semiconductor theory. This work presents a numerical simulation based on semiconductor device simulation, coupling with phase-change dynamics to simulate the electric, thermal, and phase-change characteristics for a PCM cell, and the influence of contact scaling is predicted.

This work is in three parts. First of all, the simulation principle and configurations are introduced, and it is shown that the simulated results fit the measured results well. Secondly, according to the calibrated simulation configuration, programming characteristics with different contact sizes are achieved. Lastly, the factors for reducing reset current are analyzed, and the conclusion shows that it is important to choose an appropriate contact size in the structural design of PCM cells.

2. Simulation principles and configurations

PCM operates based on the phase transition between the crystalline state and the amorphous state in some phase-change materials (such as some chalcoganides). The programming operations include a reset operation and a set operation. The reset operation is based on the phase transition from a crystalline state to an amorphous state (c→a), whereas the set operation is the reverse phase transition (a→c), which includes the temperature-induced processes due to Joule heat. The numerical simulation includes three modules: an electrical module, a thermal module and a phase-change dynamics module, shown in Fig. 1. In this work, the Sentaurus TCAD tool by Synopsys is introduced, using the MSC (multi-state configuration) and PMI (physical model interface)[8].

The electrical module can be modeled by Possion's equation and the current continuity equation, as shown in Eqs. (1) and (2).

$$\nabla^2\Psi = \frac{-q}{\varepsilon}(n - p + N_{\rm d} - N_{\rm a}), \tag{1}$$

$$\begin{cases} -q\dfrac{\partial n}{\partial t} + \nabla\cdot\boldsymbol{J}_{\rm n} = q(R_{\rm n} - G_{\rm n}), \\ q\dfrac{\partial p}{\partial t} + \nabla\cdot\boldsymbol{J}_{\rm p} = -q(R_{\rm p} - G_{\rm p}). \end{cases} \tag{2}$$

According to Eqs. (1) and (2), the Joule heat Q is calculated, as shown in Eq. (3), where $\boldsymbol{J}_{\rm n}$ and $\boldsymbol{J}_{\rm p}$ are the electron and hole current density respectively. The Joule heat is input into

* Project supported by the National Natural Science Foundation of China (No. 61176099) and the Open Project of the State Key Laboratory of Functional Materials for Informatics, China.
† Corresponding author. Email: xnlin@pkusz.edu.cn
Received 19 March 2012, revised manuscript received 11 May 2012

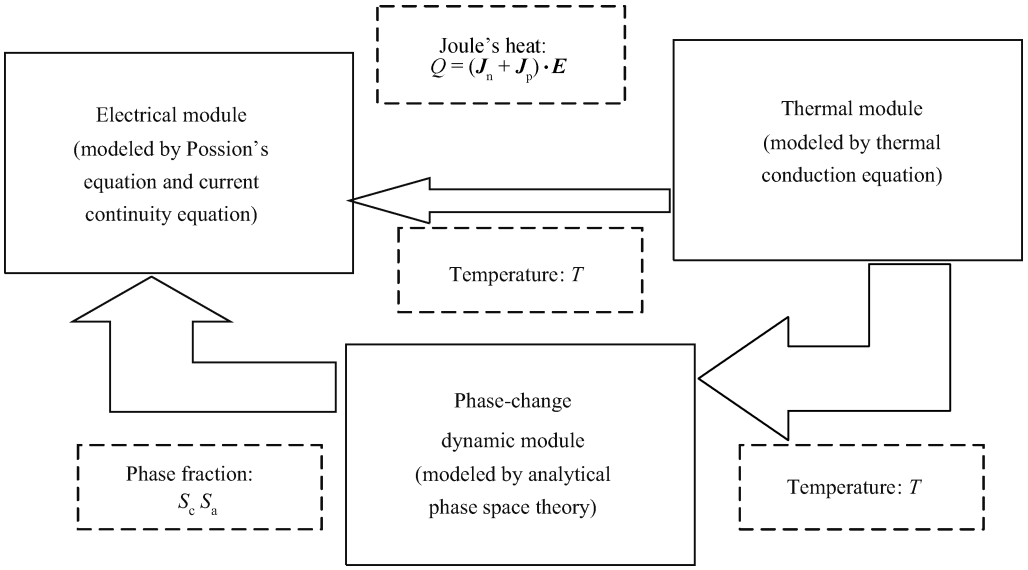

Fig. 1. Modules of the simulation.

the thermal conduction equation (Eq. (4)), and the temperature distribution of the device is achieved. Based on the temperature distribution, the thermal-induced phase-change process is simulated using an analytical phase space model[9]. According to the phase-change mechanism of phase-change materials, there are three states: crystalline state (c), amorphous state (a) and melt state (m), and the state fractions are denoted by s_c, s_a, and s_m, respectively. The summation of the state fractions satisfies Eq. (5), and the fraction of any state satisfies dynamic equation (6), where c_{ij} and e_{ij} stand for forward and backward reaction rate[9], respectively, which can be modeled by the corresponding phase-change model. In our simulation, there are three phase-change reactions: c→m, m→a, and a→c, so the fractions of the three states can be written by Eqs. (7), (8), and (9), respectively.

$$Q = (\boldsymbol{J}_n + \boldsymbol{J}_p) \cdot \boldsymbol{E}, \tag{3}$$

$$\rho c \frac{\partial T}{\partial t} = \nabla(k \cdot \nabla T) + Q, \tag{4}$$

$$\sum_i s_i = 1, \tag{5}$$

$$s_i = \sum_{j \neq i} \sum_{t \in T_{ij}} c_{ij} s_j - e_{ij} s_i, \tag{6}$$

$$s_a = c_{am} s_m - e_{ma} s_a, \tag{7}$$

$$s_c = c_{ac} s_a - e_{ca} s_c, \tag{8}$$

$$s_m = 1 - s_c - s_a. \tag{9}$$

The c→m transition and m→a transition are modeled by the Arrhenius law[9], and the a→c transition (c_{ac}) is modeled by the nucleation/growth (N/G) theory[9−11], including the nucleation rate and the growth rate model. The nucleation rate can be modeled by Eqs. (10), (11), and (12).

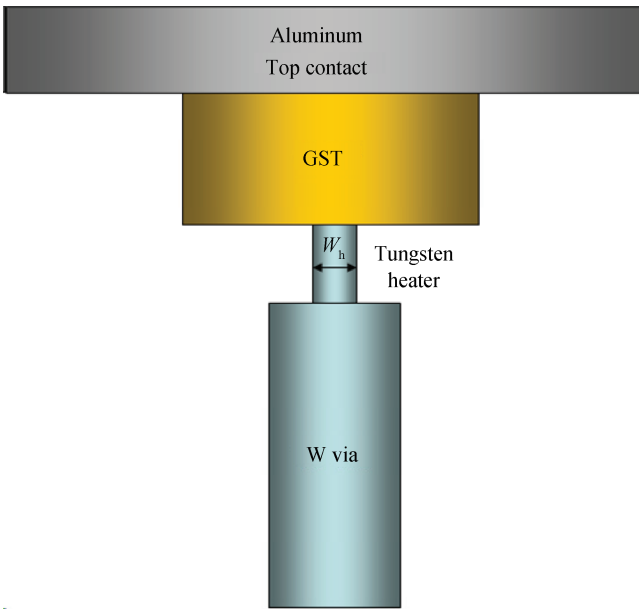

Fig. 2. Structure of PCM cell.

$$c_N = r_0 \exp\left(-\frac{E_{act} + \Delta G^*(T)}{kT}\right), \tag{10}$$

$$\Delta G^*(T) = \frac{16}{3} \frac{\pi \gamma_{SL}}{\Delta G(T)^2}, \tag{11}$$

where r_0, $\Delta G^*(T)$, ΔG, γ_{SL}, E_{act} are frequency factor, nucleation barrier, bulk free energy density, interfacial free energy, and activation energy, respectively. The growth rate is modeled by Eq. (12).

$$c_G = r_0^G \exp\left(-\frac{E_{act}^G}{kT}\right)\left[1 - \exp\left(-\frac{\Delta G(T)}{kT}\right)\right], \tag{12}$$

where r_0^G and E_{act}^G are growth frequency factor and growth activation energy.

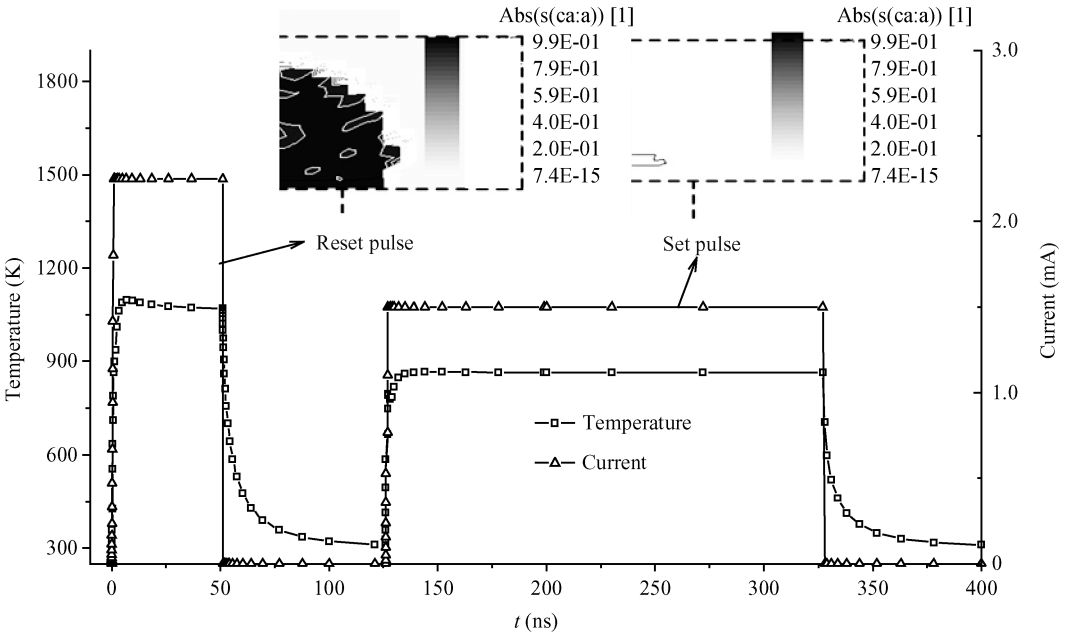

Fig. 3. Reset current pulse curve and temperature curve. The corresponding phase distribution profile is shown in the inset.

Coupling the temperature from the thermal module and the phase-change dynamic models, the fractions of every state are achieved. According to the state fraction, the mobility of carriers in phase-change material is modeled by a linear relationship. It is noted that the mobility of a carrier in an amorphous state is much lower than in a crystal state, and this character defines whether the phase-change material exhibits high or low electrical resistivity in an amorphous state or a crystal state.

$$\mu(T) = s_{\mathrm{c}}\mu^{\mathrm{c}}(T) + \mu^{\mathrm{a}}(T)(1 - s_{\mathrm{c}}). \tag{13}$$

3. Results and discussion

In our work, the structure of the PCM cell is shown in Fig. 2. The cell consists of an aluminum top contact, an active area ($Ge_2Sb_2Te_5$, namely GST), and a cylindrical tungsten heater with a diameter (W_{h}) of 70 nm. All the material parameters are acquired from Refs. [5, 9–11].

The curves of the programming pulse and temperature are shown in Fig. 3. The reset current pulse with amplitude of 2.25 mA and duration of 50 ns is loaded on the top contact firstly, and the temperature reaches about 1100 K, much higher than the melting point of GST ($T_{\mathrm{m}} = 889$ K). From the inset of Fig. 3, on the left, we can see that the fraction of the crystal state reaches about zero in the mush-like active programming area, which means that the reset process is accomplished. Following the reset current pulse, the set current pulse with amplitude of 1.5 mA and duration of 200 ns is loaded, and the corresponding temperature is about 860 K, less than the melting temperature (T_{m}), and higher than the glass temperature (T_{g}). The amorphous state transits to a crystal state induced by heating, as shown in the inset of Fig. 3, on the right.

Following the programming pulses, a read pulse is loaded on the PCM cell, whose amplitude is in the order of hundreds of μA. The amplitude of the read current pulse is so low that the temperature variation is too small to induce phase-change,

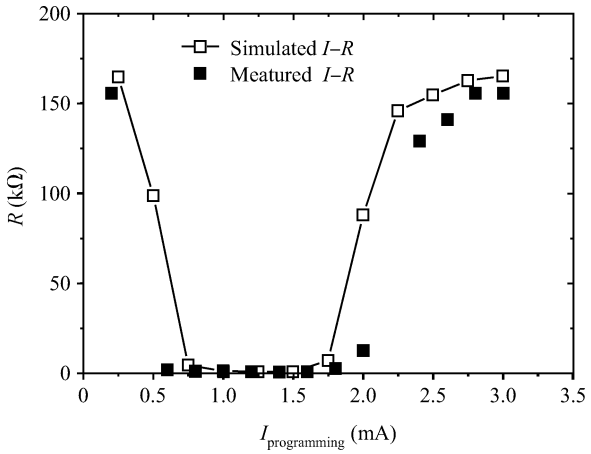

Fig. 4. Simulated and measured I–R curves.

and the reset resist and the set resist can be calculated through solving the Poission equation and current continuity equation. Under the same initial reset condition, different programming pulses with different amplitudes and the same duration are loaded, and the I–R curve is achieved, as shown in Fig. 4, and the result shows that the simulated results fit the measured data well. It is convincing that this simulation method can be used to predict the performance of a PCM cell.

For the limit of the driving capability of the access device, such as an MOSFET or a diode, it is important to optimize the structure to reduce the programming current. Based on the mechanism of the PCM, the reset and set operations are thermal driving, so enhancing the heating efficiency reduces the programming current. According to Eq. (4), there are two ways to enhance the heating efficiency. One is increasing the heat generating power; the other is reducing thermal dissipation. To increase heat generation power, according to Eq. (3), the heat generation power is proportional to current density,

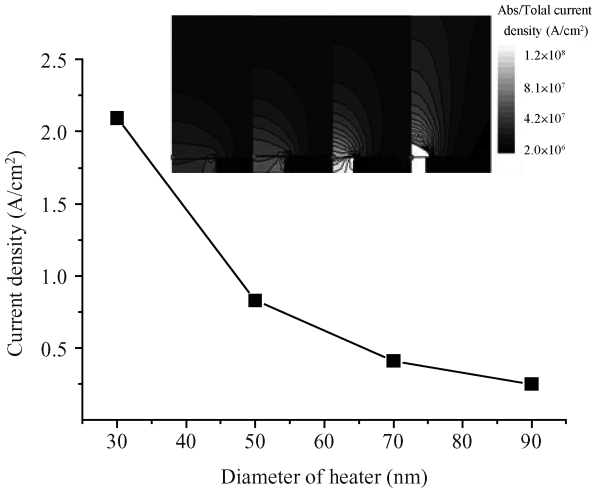

Fig. 5. Current density with different heater radii W_h = 30, 50, 70, 90 nm.

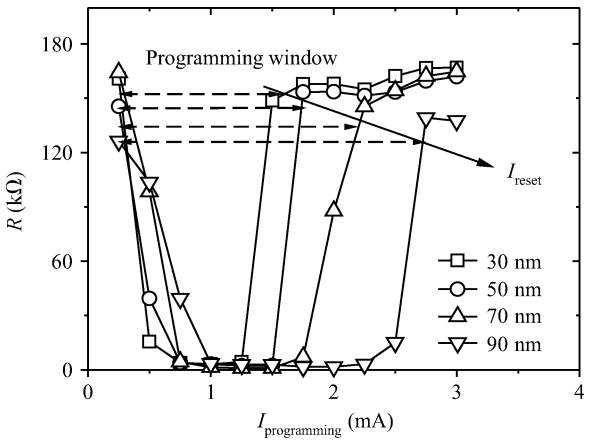

Fig. 6. $I-R$ curves with different heater sizes.

so it is reasonable to increase current density for the goal of increasing heat power. To reduce the thermal dissipation, materials with a lower thermal conductivity coefficient should be selected. In our design, for technical reasons it is difficult to change the material, therefore the method used for enhancing heating efficiency to reduce programming current focuses on increasing the heat power. Loaded by a current pulse, the current flows from the top contact, along the GST and tungsten heater to W, as shown in Fig. 1. The current is crowded in the tungsten heater. Using the same current, a smaller diameter of tungsten heater will increase the current density in a tungsten heater because of the current crowding effect. The current density curve with different W_h is shown in Fig. 5, where the current density probe points are localized in the center at the top of the heater, as shown in the inset of Fig. 5. The diameters of the heater are 30, 50, 70, and 90 nm, respectively. We can see that the current density increases with the reduction of W_h. The $I-R$ curve with different W_h is shown in Fig. 6. From Fig. 6, the curves of I_{reset} versus W_h can be achieved, as shown in Fig. 7. Through Fig. 6, on one hand, it is shown that the reset current increases along with the increment of the size of heater; on the other hand, as shown by the range labeled by a dashed line arrow in Fig. 6, the programming window displays a decreasing trend along with the decrease of the heater diameter, which can be explained by the decrease of thermal power generation along with the increase of heater size. The reset currents and the programming window are shown in Fig 7. Through Fig. 7, it is shown that the reset current is approximately proportional to the diameter of the heater, and the programming window has the same trend. The above results imply that the selection of an appropriate heater size is a key factor for optimizing the performance of a phase-change memory cell. To reduce the power consumption of the phase-change memory, it is important to reduce the reset current, which means the reduction of the heater size. In addition, reducing the heater size also reduces the programming window, which leads to difficulties in the design of the peripheral circuits. In summary, the design of a phase-change memory structure is a trade-off job.

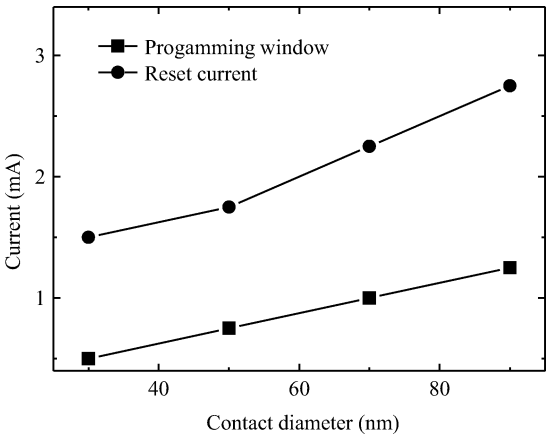

Fig. 7. Reset currents and programming widows with different heater sizes.

4. Conclusion

In summary, this letter provides a simulation method for phase-change memory. This simulation is based on semiconductor theory to model the electric–thermal coupling process, which is more adaptable for the characteristics of phase-change materials. This simulation can achieve transient temperature distribution and phase distribution. $I-R$ results show that this simulation method is an efficient method to predict the performance of a PCM cell. Using this simulation, the key factor for the phase-change memory design is implemented, which is used to optimize the phase-change memory cell structure.

Acknowledgement

We would like to thank Mr. Jin Rong for the fruitful discussions.

References

[1] Lai S. Current status of the phase change memory and its future. IEEE International Electron Devices Meeting, Technical Digest, 2003: 255

[2] Lacaita A L, Ielmini D, Mantegazza D. Status and challenges of phase change memory modeling. Solid-State Electron, 2008,

52(9): 1443
[3] Xu Cheng, Liu Bo, Chen Yifeng. Switching characteristics of phase change memory cell integrated with metal–oxide–semiconductor field effect transistor. Chin Phys Lett, 2008, 25(5): 1848
[4] Feng Gaoming, Liu Bo, Wu Liangcai, et al. Properties of W submicrotube heater electrode used for phase change memory. Chinese Journal of Semiconductors, 2007, 28(7): 1134
[5] Kim D H, Merget F, Först M, et al. Three-dimensional simulation model of switching dynamics in phase change random access memory cells. J Appl Phys, 2007, 101(6): 064512
[6] Http://ovonyx.com/technology/technology.com
[7] Gong Yuefeng, Song Zhitang, Ling Yun, et al. Simulation of voltage SET operation in phase-change random access memories with heater addition and ring-type contactor for low-power consumption by finite element modeling. Chin Phys Lett, 2010, 27(6): 068501
[8] Sentaurus Device User Guide, Version A-2007.12, Dec. 2007
[9] Schmithusen B, Tikhomirov P, Lyumkis E. Phase-change memory simulations using an analytical phase space model. SISPAD: International Conference on Simulation of Semiconductor Processes and Devices, 2008: 57
[10] Peng C, Cheng L, Mansuripur M. Experimental and theoretical investigations of laser-induced crystallization and amorphization in phase-change optical recording media. J Appl Phys, 1997, 82(9): 4283
[11] Wei Y, Wang L, Wang W. Numerical simulation of programming and read process for nano-scaled phase-change memory (PCM) cell. IEEE International Conference of Electron Devices and Solid-State Circuits, EDSSC, 2009: 529